Title

Three-dimensional non-destructive optical evaluation of laser-processing performance using optical coherence tomography

Journal

Optics & Laser Technology, 40(4)

ISSN

0030-3992

Authors

Kim, Youngseop
Choi, Eun Seo
Kwak, Wooseop
et al.

Publication Date

2008-06-01

DOI

10.1016/j.optlastec.2007.09.011

HHS Public Access

Author manuscript

Opt Laser Technol. Author manuscript; available in PMC 2014 June 11.

Published in final edited form as:

Opt Laser Technol. 2008 June 1; 40(4): 625–631. doi:10.1016/j.optlastec.2007.09.011.

Three-dimensional non-destructive optical evaluation of laser-processing performance using optical coherence tomography

Youngseop Kim[a], **Eun Seo Choi**[a,*], **Wooseop Kwak**[a], **Yongjin Shin**[a], **Woonggyu Jung**[b], **Yeh-Chan Ahn**[b], and **Zhongping Chen**[b]

[a]Laser Imaging Laboratory and Department of Physics, Chosun University, 375 Seosuk-dong, Dong-gu, Gwangju 501-759, Republic of Korea

[b]Beckman Laser Institute and Department of Biomedical Engineering, University of California at Irvine, Irvine, CA 92612, USA

Abstract

We demonstrate the use of optical coherence tomography (OCT) as a non-destructive diagnostic tool for evaluating laser-processing performance by imaging the features of a pit and a rim. A pit formed on a material at different laser-processing conditions is imaged using both a conventional scanning electron microscope (SEM) and OCT. Then using corresponding images, the geometrical characteristics of the pit are analyzed and compared. From the results, we could verify the feasibility and the potential of the application of OCT to the monitoring of the laser-processing performance.

Keywords

Optical coherence tomography (OCT); Non-destructive diagnosis; Laser marking

1. Introduction

The development of ultra-short pulse lasers has increased the fundamental understanding of interaction behaviors between a laser beam and a material, and the advance of a high-power laser technology has facilitated technical developments in laser-based material processing. With the development of high-powered and short-pulsed lasers, conventional material processing typically done using mechanical tools has instead been performed by commercial-grade lasers such as CO_2 and Nd:YAG lasers, providing advantages of cost-effectiveness, high precision and non-contact processing [1,2].

Though the laser-based material processing has the potential to present a high degree of freedom in the control of fabrication processes, unwanted sample deformations commonly occur during various laser processing such as engraving, marking, cutting, bending, and welding due to the improper usage of laser irradiation conditions. To prevent quality degradation of the laser processing, many researchers have focused on the development of

*Corresponding author. Tel.: +8262 230 6678; fax: +8262 225 6659. cesman@chosun.ac.kr (E. Seo Choi).

diagnostic techniques by employing optical, acoustic, thermal, and computational methods. For instance, an acoustic wave may be used as a means of detecting the condition of a weld in a workpiece [3]; the acoustic wave originates from the shockwave created when a plume is rapidly expanded during the welding process. A pyrometer, an infrared radiation sensor, is used to monitor surface temperature variation in laser brazing [4]. In addition, laser-induced ultrasonic waves show great potential for use in the examination of welding conditions [5]; the application of a voltage or a current Hall effect transducer is also available for monitoring welding conditions [6]. Other, more commonly exploited monitoring methods include optical and visible approaches.

Optical inspection methods for laser processing have generally utilized a photodiode or photodiode array with light sources ranging from UV to IR [7]. In many cases, the plasma caused by a highly focused laser beam is measured using optical inspection methods, and the information of sputter and bead shape could be obtained from this measurement [8]. The spectral response to a different colored light source, which is dependent on the welding condition, has been measured and analyzed to determine the correlation between a processing mechanism and an optical signal variation. In addition, spectrally analyzed information obtained using laser spectroscopy [9,10] such as laser-induced breakdown spectroscopy and laser-induced fluorescence spectroscopy has been used to monitor the quality of a laser-based cleaning processing.

Compared with the above approaches, visual methods utilizing a CMOS or CCD camera can acquire more comprehensive information regarding surface deformations [11]. Although direct observations using an optical microscope or other visual methods can be used to view a three-dimensional profile of a laser-processing region, it is difficult to analyze the two-dimensional cross-sectional or three-dimensional structural information of deeply engraved samples because of limitations in observable depth. Though the prior methods could be applied to investigate laser processing, a more precise evaluation of laser-based processing performance is required before a cross-sectional view of physically bisected workpiece can be observed; to this end an optical microscope or a scanning electron microscope (SEM) is suggested [12]. However, a physically bisected workpiece would probably reveal distorted results based on the fact that it is likely that the workpiece would be damaged or spoiled during the cutting process. Another disadvantage is that this method could not be applied to the real-time monitoring of the laser-based processing and could require a time-consuming preparation process.

As a promising optical imaging modality, optical coherence tomography (OCT) has the potential to provide a high-resolution non-destructive cross-sectional image by using a white-light interferometry scheme [13–15]. The use of a white-light or broadband source provides a high axial spatial resolution of up to submicrons, achieved by coherence gating. The exploitation of interference effects makes it possible have a measurement range of up to several millimeters along the depth of a sample. Using an optical scanner over the sample, OCT could reconstruct the cross-sectional image of the sample without any incision. When the detailed tomography of a sample is obtained, OCT does not require any physical contact or destruction of the sample. Until now, most interest in OCT research has been focused on the *in vivo* imaging of biomedical samples of retinas [16], skin [17], and blood vessels [18].

In spite of fewer applications in material characterization, as compared with OCT use in biomedical fields, the application of OCT for the non-destructive imaging and examination of non-biomedical samples has continuously increased due to inherent advantages of OCT; the ability to view the resolvable anatomy of biological tissues at a micron-scale.

In many cases, the primary task of an OCT application is the imaging of structural information. For instance, results pertaining to the detection or examination of the subsurface cracks in the material of ceramics have been reported [19]. The imaging of the internal microstructures of polymer matrix [20], injection-molded plastic parts [21], and paper [22] has also been demonstrated. Besides conventional cross-sectional imaging, the functional imaging of a strain-mapping required for the stress analysis has also been presented using polarization-sensitive OCT [23].

In this paper, we present our results related to the use of OCT to monitor the performance of the laser processing of an acrylonitrile butadiene styrene (ABS) plastic. ABS plastic is currently widely used in numerous applications, but due to its high thermal sensitivity, the performance of laser processing on an ABS plastic sample can be significantly degraded when improper irradiation conditions are applied. For these reasons, the monitoring of the performance of laser processing is required as part of the investigation into how to optimize processing conditions.

In the investigation of performance variation in a sample, an ABS plastic having high sensitivity to laser operational conditions is selected as the most appropriate material. Initially, the ABS plastic sample used in the experiment has a plane surface with high reflectivity. Though various plastics have been imaged using an OCT system, it is rare to find OCT images of laser-processed plastics that were used for an evaluation of laser-processing performance. Previously, the cross-sectional images of the surface deformation formed on an glass and ABS plastic samples by laser processing were reported [24,25]. Also, microscopic images of pits and rims on an ABS plastic created by a Q-switched Nd:YAG laser were compared with the corresponding OCT images, which were found to be well matched [25].

However, more detailed analysis of the laser processing on materials such as a change in geometrical shape, an increase in depth, and rim formation of a pit due to laser-processing conditions have not yet been performed. To appreciate the difference in the laser-processing performance for different processing conditions, we performed OCT imaging on a number of samples while changing operational parameters such as pulse energy and the repetition rate of a Q-switched Nd:YAG pulse laser; this laser is commonly used for laser processing in industrial and clinical fields [26]. By reconstructing a series of two-dimensional tomographies, we generated three-dimensional images of deformed samples on ABS samples deformed during laser processing. Through the presentation of these three-dimensional images, we could investigate the dependence of the laser processing on operational parameters such as single pulse energy, repetition rates, and number of pulses, factors that were used to explain why the laser-processing performance of identical materials may vary. Then, we compared the OCT images to SEM images.

Although in previous studies, two-dimensional images obtained with a time-domain OCT system are presented, in this paper we present three-dimensional image to enhance the availability of information integrated from the two-dimensional OCT images. And although a quantitative analysis is not dealt with in the paper, more plentiful information for evaluating laser-processing performance can be analyzed. Finally, contrary to other papers [22,25], this paper employs laser processing using a pulse laser, which displays a significantly smaller pit and rim size.

2. Experiment and results

Fig. 1 shows the schematic diagram of a laser-processing system. In laser-based material processing, we used a Q-switched Nd:YAG pulse laser operating at 1064 nm with an 8 ns pulse width, which is defined as the full width at half maximum (FWHM) of a temporal pulse shape.

During experiment, the pulse energy and repetition rate of the laser were discretely varied from 200 to 325mJ and 1 to 20Hz, respectively. The number of pulses is ranged from 1 to 40. A high power laser beam was focused on an ABS plastic sample, which was made of an ABS resin (LG AF-302) and is very popular as a data storage material, through the lens having 100mm focal length. The laser beam was then irradiated on a small spot size of 100 μm in diameter. The spot size was measured by the knife-edge method, a conventional method for measuring spot size. It was found that the surface morphology changed as the pit evolved; the evolution of the pit depends on the irradiation conditions, as is imaged by a conventional SEM and an OCT system. When the SEM images were compared with the OCT images, they showed good agreement with each other, which validates the potential of OCT imaging as an alternative inspection tool. In this experiment, we applied different operational parameters while keeping the total irradiation energy constant to investigate the laser-processing dependence on operating conditions.

A schematic of the OCT system used in this experiment is illustrated in Fig. 2 [27]. As can be seen in the figures, the laser beam from a broadband source is coupled into a 2 × 2 fiber coupler and split into a sample and a reference arm, where the ABS plastic and a nearly perfect reflector or metal-coated mirror are placed in the sample and the reference arm, respectively. As a broadband source, a broadband super-luminescent diode laser having an output power of 10mW at a central wavelength of 1310 nm with a bandwidth of 95nm was used; which corresponds to 8 μm in axial resolution. A visible aiming beam (633 nm) was used to locate the exact imaging position on the ABS plastic sample. The reflected beam from the two arms of the interferometer was recombined in the fiber coupler and made an interference signal dependent on an optical pathlength difference between the two arms, and this signal was then directed to a spectrometer. The dispersed spectrum was sampled by the spectrometer with a 1 × 1024 InGaAs detector array at 7.7 kHz. Here, the spectral range of the array was 130 nm, which corresponds to a spectral resolution of 0.13nm and an imaging depth of 3.4mm in air.

In the sample arm, the collimated beam from a fiber type collimator was focused on the ABS plastic through the objective lens. In order to reconstruct a three-dimensional image by

using a series of two-dimensional images, additional scanning on the sample was performed by a two-axis scanner. A probing beam with a 15 μm spot size at the focal point was then focused on our sample. The position of the visible beam could be adjusted to accurately place the point of the probing beam. In this way, the OCT system was used to provide real-time cross-sectional imaging of the sample, and the volumetric image could be presented within a few seconds, though the processing time required changed depending on the size of an image to be obtained.

Fig. 3 shows the top-view SEM images of a series of pits formed on the ABS plastic through the variation of laser irradiation conditions; the total irradiation energy used was 100, 2000, and 4000 mJ, respectively. When deformation of the surface of the ABS plastic started at the lowest irradiation energy, no significant pit or rim formation was observed, as shown in Fig. 3(a). For a single pulse, the surface of the crater is very rough, with the diameter is less than 500 μm. As the irradiation energy was increased to 200 mJ, the radius and the depth of the pit correspondingly increased, as shown in Fig. 3(b). For 20 pulses, it can be seen that the crater diameter is larger than 500 μm and the surface shows polymer clumping. Finally, at irradiation energy of 4000 mJ, the overall shape of the pit is totally different from the results obtained for 2000 mJ. For 40 pulses, the crater diameter is larger than 1mm and elliptical deformation is apparent. The surface roughness seen in Fig. 3(c) is smoother than that seen in Fig. 3(b) as the melting effect due to the energy accumulation is the dominant factor in pit formation. During irradiation, the maximum measured surface temperature of the ABS plastic was less than 2000 K. Thus, the plasma formation was not expected at the focal point or above the surface of the ABS plastic. Due to the slow heat diffusion of the ABS plastic, the accumulation of heat at the focal point seemed to depend on the number of pulses, which was thus responsible for a smoother surface at 40 pulses. The competition between heat diffusion and the repetition rate ultimately decided the smoothness of the crater. These results reveal that the surface deformation of ABS plastic is strongly dependent on the total irradiation energy during laser processing. We also believe that the different laser irradiation conditions at the same total energy incur different crater shapes.

Figs. 4 and 5 present the OCT imaging results from the top view, the cross-sectional view and three-dimensional view of the pit. Fig. 4 shows OCT images obtained from the ABS plastic shown in Fig. 3(b). It can be seen that the top-view image of the pit in Fig. 4(b) is well matched with its corresponding SEM image. The three-dimensional image in Fig. 4(c), reconstructed by a series of cross-sectional images, clearly presents the morphology of the rim around the pit. Thus, it was possible to examine the shape and the depth of the pit formed during the laser processing using the OCT system, without incurring any damage to the sample. Fig. 4(d) demonstrates that it is indeed feasible to use OCT as a non-destructive monitoring tool.

From Fig. 5, we can understand that the differences in pit growth are dependent on the total irradiation energy. The elliptical shape of the top surface of the pit in Fig. 5(a) and (b) are in exact agreement with each other. This result is also well matched with the result provided in Ref. [28], where it was shown that the direction of the major axis in the elliptic rim has a tendency to align in the direction of ABS resin ejection. From repeated experiments with changing the sample directions, we could verify that beam distortion is not a main cause of

elliptical deformation. The ABS plastic sample was made by ejecting a melted resin through a nozzle. As the hot resin cooled, stress along the ejection direction in the sample remained. When the sample was irradiated by a laser pulse, this stress was released, as is evident by the formation of an asymmetric shape [28]. The three-dimensional pit shape in Fig. 5(c) and the cross-sectional view in Fig. 5(d) show that the depth and radius of the pit become deeper and larger as the total irradiation energy increases during laser processing.

A series of OCT images in Fig. 6, obtained by optical scanning, are sequentially arranged along the scanning direction. The volume image at the center of Fig. 6 is also made using these two-dimensional tomograms. The sequential arrangement of the images allowed for the fuller understanding of the overall shape of the pit, which shows symmetric deformation and depth variation of the pit is very abrupt because the slope in the pit is very steep. In our experiment, we changed the lateral scanning speeds to vary lateral resolution, and determined that the lateral scanning resolution is sufficient for imaging the steep slope of the crater. As in the cut view of the sample, we also observed the same slope of the crater. Another interesting feature observed is that compared with the pit bottom in Fig. 6(6 and 8) (designated with arrow) show that the center or the bottom of the pit is slightly lifted because of the recoil pressure effect during laser processing.

OCT imaging could clearly visualize the detailed surface morphology of the pit, as shown in Fig. 7. When compared with the SEM imaging results shown in Fig. 7(b), the OCT images displayed very similar surface roughness. For a more detailed view, the SEM and OCT images are magnified by five times. However, under this level of magnification, it became very difficult to quantitatively compare the SEM image to the OCT image, as the resolution of the OCT system is significantly lower than for SEM. However, the images obtained by the OCT system can still illustrate the trend of change in the morphology of the crater surface.

3. Conclusion

In this paper, we performed laser processing on an ABS plastic as the total irradiation energy was varied. In the evaluation of the results of laser processing, we utilized a conventional SEM imaging method and the optical imaging method OCT. During experimentation, we focused our observation on the laser-processing results pertaining to the features of pit and rim formation, as shown in the SEM images. Then, we confirmed that the OCT images, obtained by optical sectioning without requiring the physical destruction of the ABS plastic, presented good agreement with the SEM analysis results. It was found that at higher total irradiation energy there was greater elliptical deformation of the rim, increased pit depth, and surface roughness improvement, where the surface roughness was evaluated not quantitatively but qualitatively. In this way, we compared and verified the trends shown in both SEM and OCT images.

However, results of this study show that the lateral resolution of OCT is not sufficient for imaging an object a couple of microns in size. This restriction of lateral resolution originates from the diffraction limit of the optics used in OCT systems. For this reason, we focused not

on the sophisticated calculation of micro-structural variation but on the macroscopic "real-time monitoring" of pit formation without bisecting the samples.

From these results, we could confirm that the application of OCT to the monitoring of the laser processing is very promising. We found that the performance of laser processing could be evaluated without any physical sectioning or preprocessing techniques such as chamber under vacuum and sample coating.

Three-dimensional images have the potential to provide all pit information, including geometrical asymmetry, geometrical distortions, calculation of a pit volume, and analysis of beam quality required for laser processing. We expect that real-time monitoring and evaluation of the laser-processing performance can be possible with the integration of an OCT system with a high-power pulse laser.

References

1. Lee JY, Ko SH, Farson DF, Yoo CD. Mechanism of keyhole formation and stability in stationary laser welding. J Phys D: Appl Phys. 2002; 35:1570–1576.
2. Mikhail I, Martin W, Said A, Manfred K, Peter H. Ablation of hard bone tissue with pulsed CO_2 lasers. Med Laser Appl. 2005; 20:13–23.
3. Li L. A comparative study of ultrasound emission characteristics in laser processing. Appl Surf Sci. 2002; 186:604–610.
4. Jeon M, Kim W, Han G, Na S. A study on heat flow and temperature monitoring in the laser brazing of a pin-to-plate joint. J Mater Process Technol. 1998; 82:53–60.
5. Miller M, Mi B, Kita A, Ume C. Development of automated real-time data acquisition system for robotic weld quality monitoring. Mechantronics. 2002; 12:1259–1269.
6. Wang Y, Chen Q. On-line quality monitoring in plasma-arc welding. J Mater Process Technol. 2002; 120:270–274.
7. Zhang X, Chen W, Ashida E, Matsuda F. Relationship between weld quality and optical emissions in underwater Nd:YAG laser welding. Opt Laser Eng. 2004; 41:717–730.
8. Park H, Rhee S. Estimation of weld bead size in CO_2. J Laser Appl. 1999; 11:143–150.
9. Anglos, D.; Couris, S.; Mavromanolakis, A. Artwork diagnostics: laser induced breakdown spectroscopy (LIBS) and laser induced florescence (LIF) spectroscopy. Proceedings of the first international conference on lasers in the conservation of artworks; Heraklion, Greece; 1995. p. 113-118.
10. Fotakis C. Lasers for art's sake. Opt Photon News. 1995; 6:30–35.
11. Zhang Y, Kovacevic R, Li L. Characterization and real-time measurement of geometrical appearance of the weld pool. Int J Mach Tool Manufact. 1998; 36:799–816.
12. Yung KC, Mei SM, Yue TM. A study of the heat-affected zone in the UV YAG laser drilling of GFRP material. J Mater Process Technol. 2002; 122:278–285.
13. Huang D, Swanson EA, Lin CP, Schuman JS, Stinson WG, et al. Optical coherence tomography. Science. 1991; 254:1178–1181. [PubMed: 1957169]
14. Fercherl AF, Drexler W, Hitzenberger CK, Lasser T. Optical coherence tomography-principles and applications. Rep Prog Phys. 2003; 66:239–303.
15. Bouma, BE.; Tearney, GJ. Handbook of optical coherence tomography. 1st ed. New York: Dekker; 2002.
16. Puliafito A, Hee MR, Lin CP, Reichel E, Schuman JS, et al. Imaging of macular diseases with optical coherence tomography. Ophthalmology. 1995; 102:217–229. [PubMed: 7862410]
17. Welzel J, Lankenau E, Birngruber R, Engelhardt R. Optical coherence tomography of the human skin. J Am Acad Dermatol. 1997; 37:958–963. [PubMed: 9418764]

18. Tearney GJ, Yabushita H, Houser SL, Aretz HT, Jang IK, et al. Quantification of macrophage content in atherosclerotic plaques by optical coherence tomography. Circulation. 2003; 107:113–119. [PubMed: 12515752]
19. Baskansky M, Duncan MD, Kahn M, Lewis D III, Reintjes J. Subsurface defect detection in ceramics by high-speed high-resolution optical coherent tomography. Opt Lett. 1997; 22:61–63. [PubMed: 18183103]
20. Dunkers JP, Parnas RS, Zimba CG, Peterson RC, Flynn KM, et al. Optical coherence tomography of glass reinforced polymer composites. Composites. 1999; A30:139–147.
21. Stifter D, Burgholzer P, Höglinger O, Götzinger E, Hitzenberger CK. Polarisation-sensitive optical coherence tomography for material characterisation and strain-field mapping. Appl Phys. 2003; A76:947–951.
22. Alarousu E, Krehut L, Prykari T, Myllyla R. Study on the use of optical coherence tomography in measurements of paper properties. Meas Sci Technol. 2005; 16:1131–1137.
23. Oh J-T, Kim S-W. Polarization-sensitive optical coherence tomography for photoelasticity testing of glass/epoxy composites. Opt Exp. 2003; 11:1669–1676.
24. Shin Y, Kim Y, Park S, Jung B, Lee J, Nelson JS. Pit and rim formation during laser marking of acrylonitrile butadiene styrene plastic. J Laser Appl. 2005; 17:243–246.
25. Wilson, JJ.; Hawkes, JFB. Laser: principles and applications. New York: Prentice-Hall International; 1987. p. 194-199.
26. Shin Y, Kim H, Kim Y, Park S, Jung W, et al. Investigation of pit formation in laser-irradiated multilayer thin films by using optical coherence tomography. J Kor Phys Soc. 2006; 48:L184–L187.
27. Ahn Y-C, Jung W, Chen Z. Turbid two-phase slug flow in a microtube: simultaneous visualization of structure and velocity field. Appl Phys Lett. 2006; 89:064109–064111.
28. Kim Y, Shin Y, Jeong G, Ryang K. Pit formation on ABS plastic by CO2 and Nd:YAG laser. New Phys. 2002; 44:305–311.

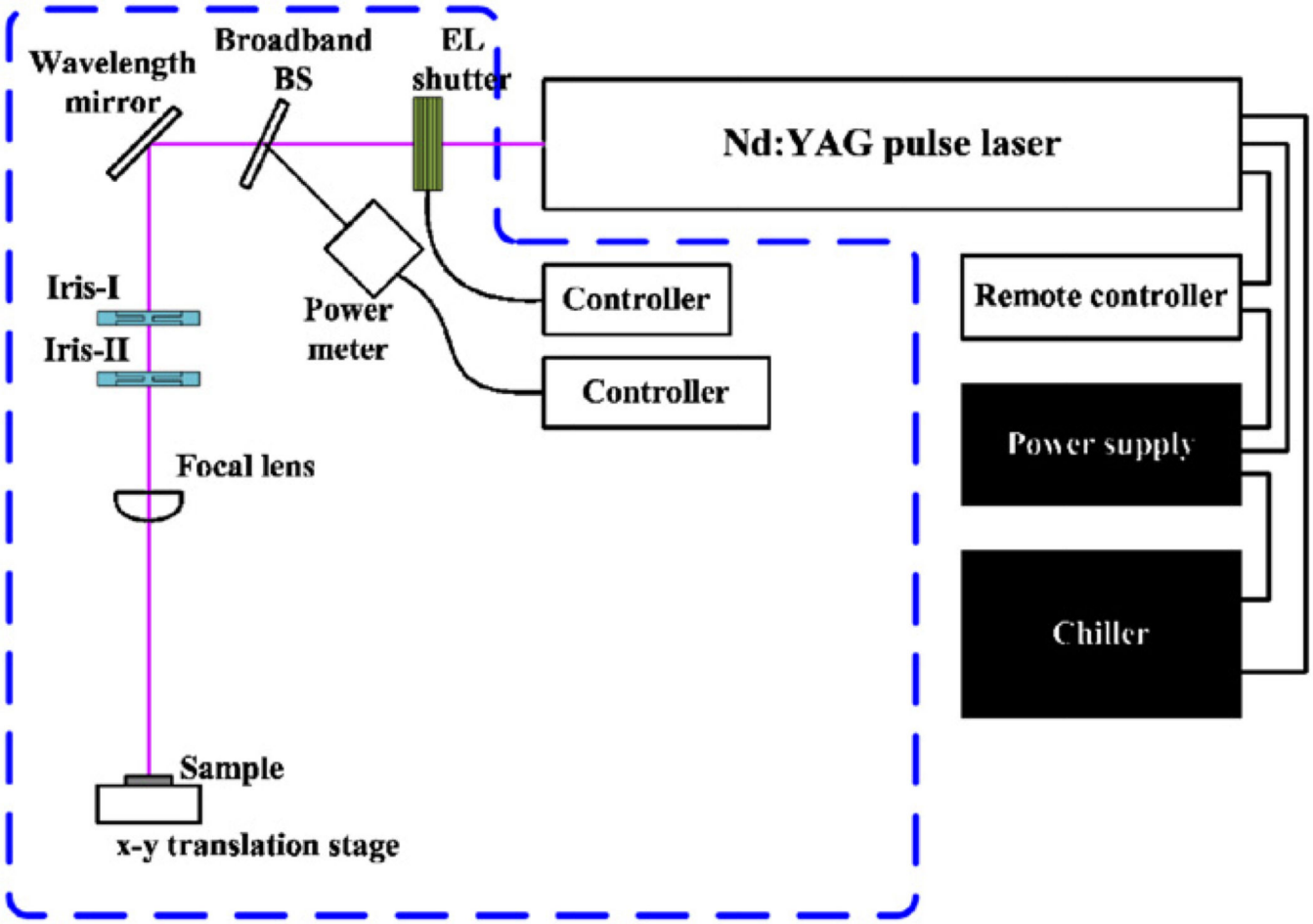

Fig. 1.

Schematic of a Q-switched Nd:YAG pulse laser-processing system. The part surrounded with dotted lines is the beam delivery system: EL shutter, electrically-controlled shutter; broadband BS, wide spectral beam splitter; wavelength mirror, dielectric mirror designed with high reflectivity at 1064 nm; focal lens, focusing lens.

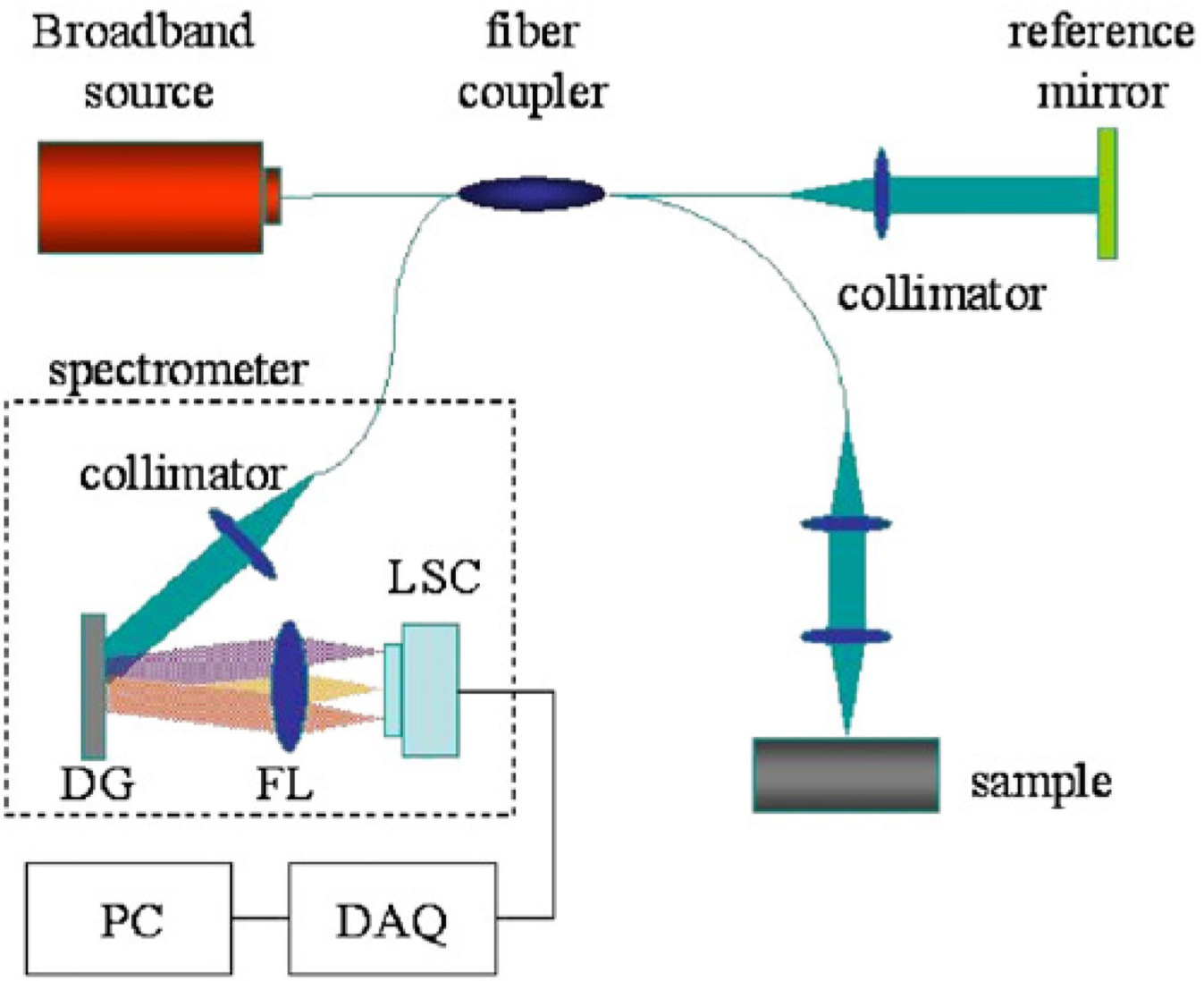

Fig. 2.
Schematic of the OCT system: DG, diffraction grating; FL, focal lens; LSC, line scan camera; DAQ, data acquisition board.

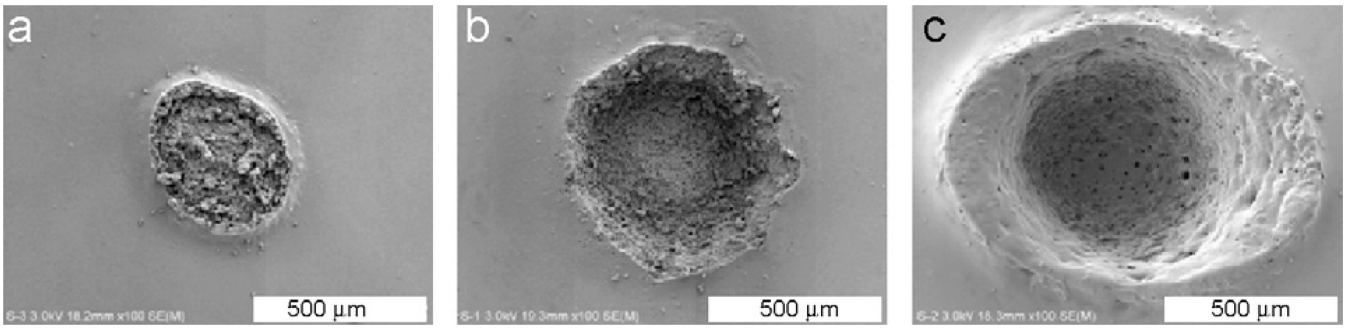

Fig. 3.

SEM images of laser-processed ABS plastic with different laser operational parameters: (a) 1 pulse at 1 Hz, (b) 20 pulses at 1 Hz, and (c) 40 pulses at 20 Hz. The energy for a single pulse is fixed at 100 mJ.

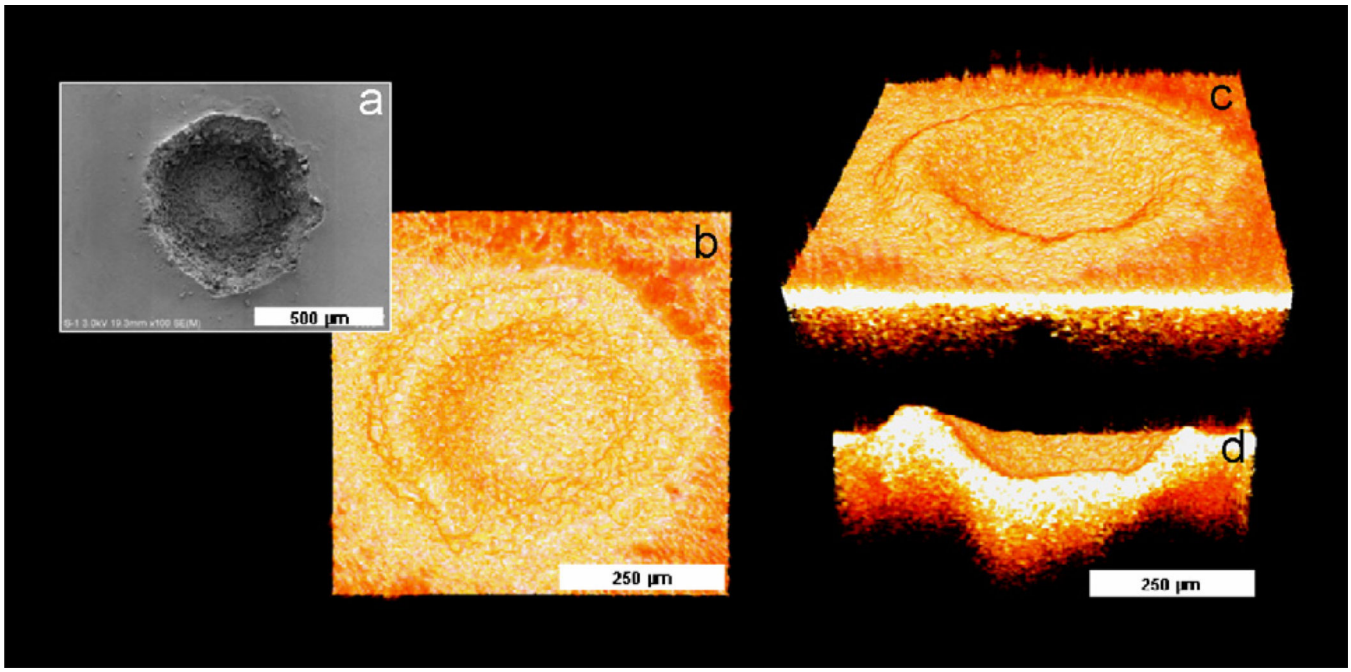

Fig. 4.

SEM and OCT images of laser-processed ABS plastic formed under the laser operational condition of 20 pulses at 1Hz (2000 mJ). (a) The top-view SEM image, (b) the top-view OCT image, (c) the reconstructed three-dimensional OCT image, and (d) the cross-sectional OCT image at the center of the sample.

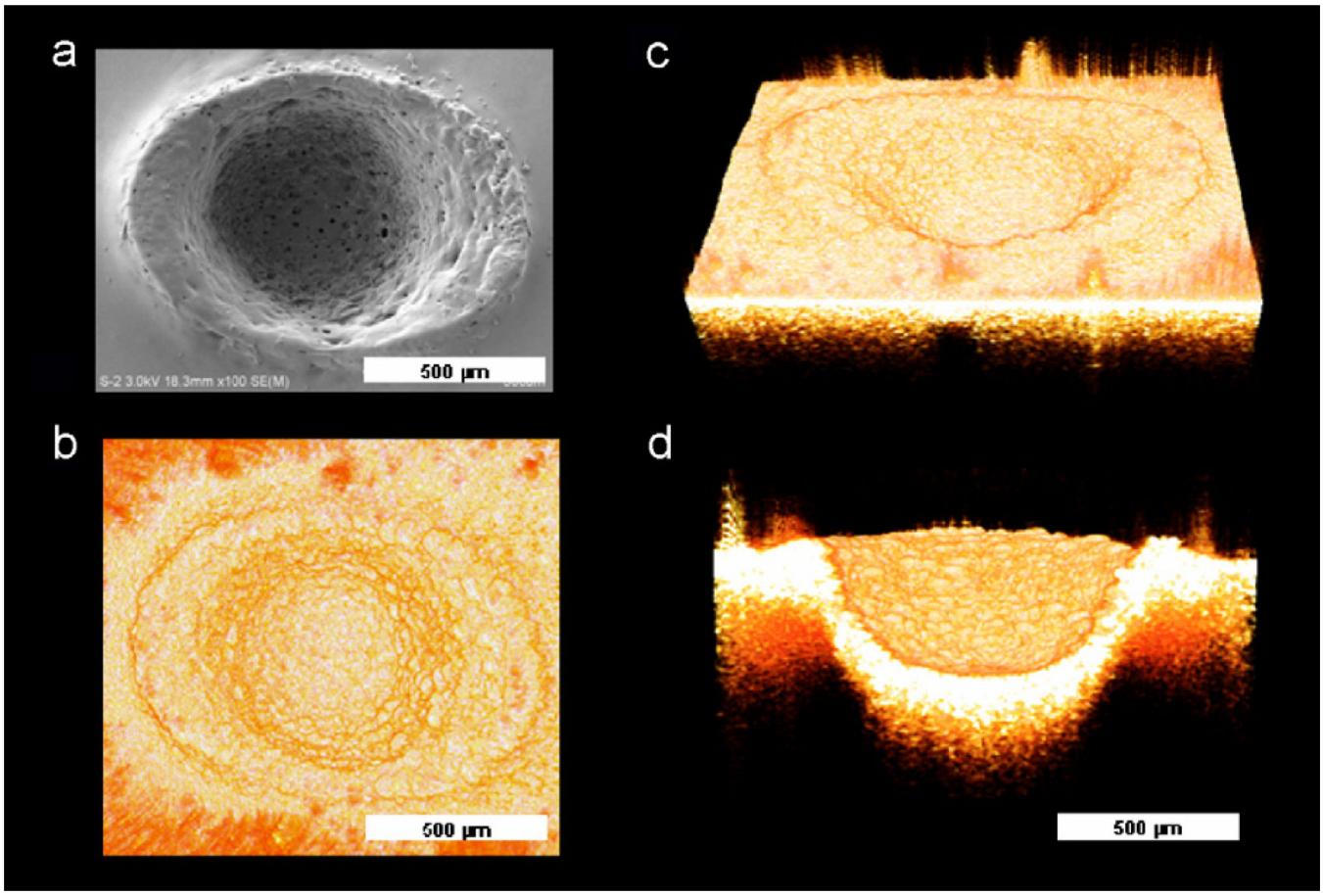

Fig. 5.

SEM and OCT images of laser-processed ABS plastic formed under the laser operational condition of 40 pulses at 20 Hz (4000 mJ). (a) The top-view SEM image, (b) the top-view OCT image, (c) the reconstructed three-dimensional OCT image, and (d) the cross-sectional OCT image at the center of the sample.

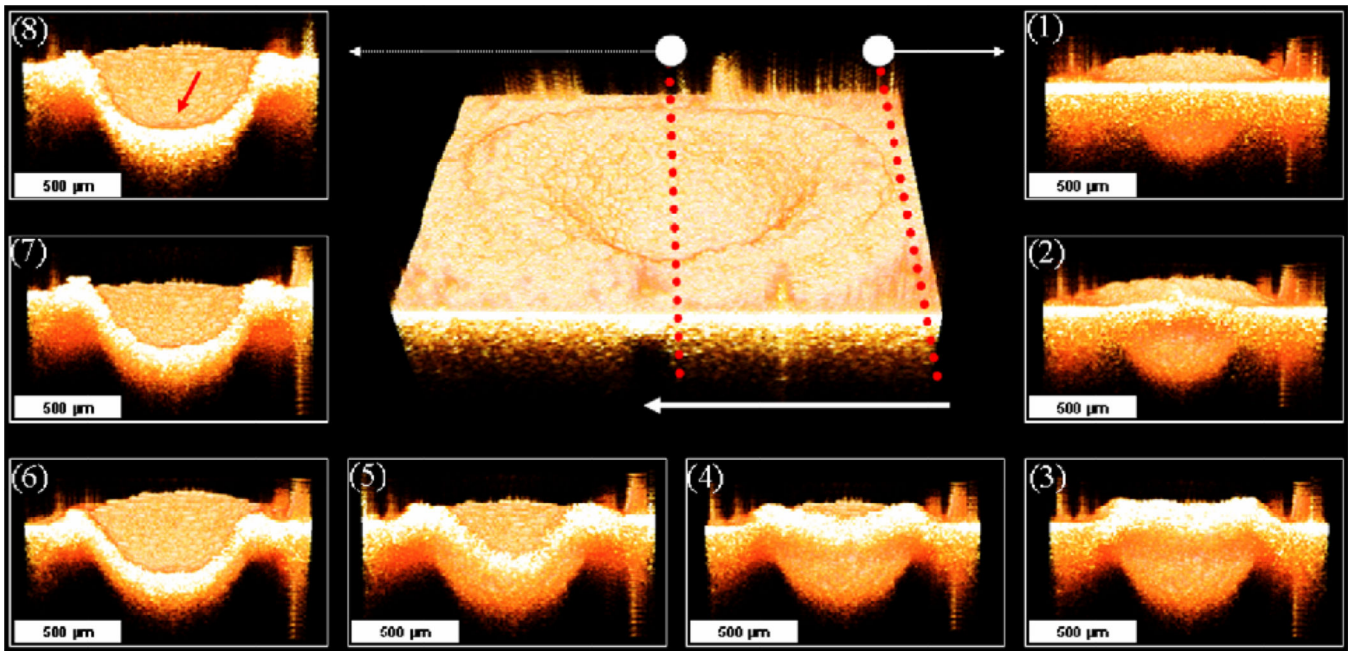

Fig. 6.

A series of OCT images obtained by the scanning from the right (1) to the left (8) direction across the ABS plastic under the laser operational condition of 40 pulses at 20 Hz (4000 mJ). The arrow shown in the center three-dimensional OCT image expresses the direction of scanning from (1) to (8). An arrow in (8) indicates a portion of the pit that lifted up due to recoil pressure during laser processing.

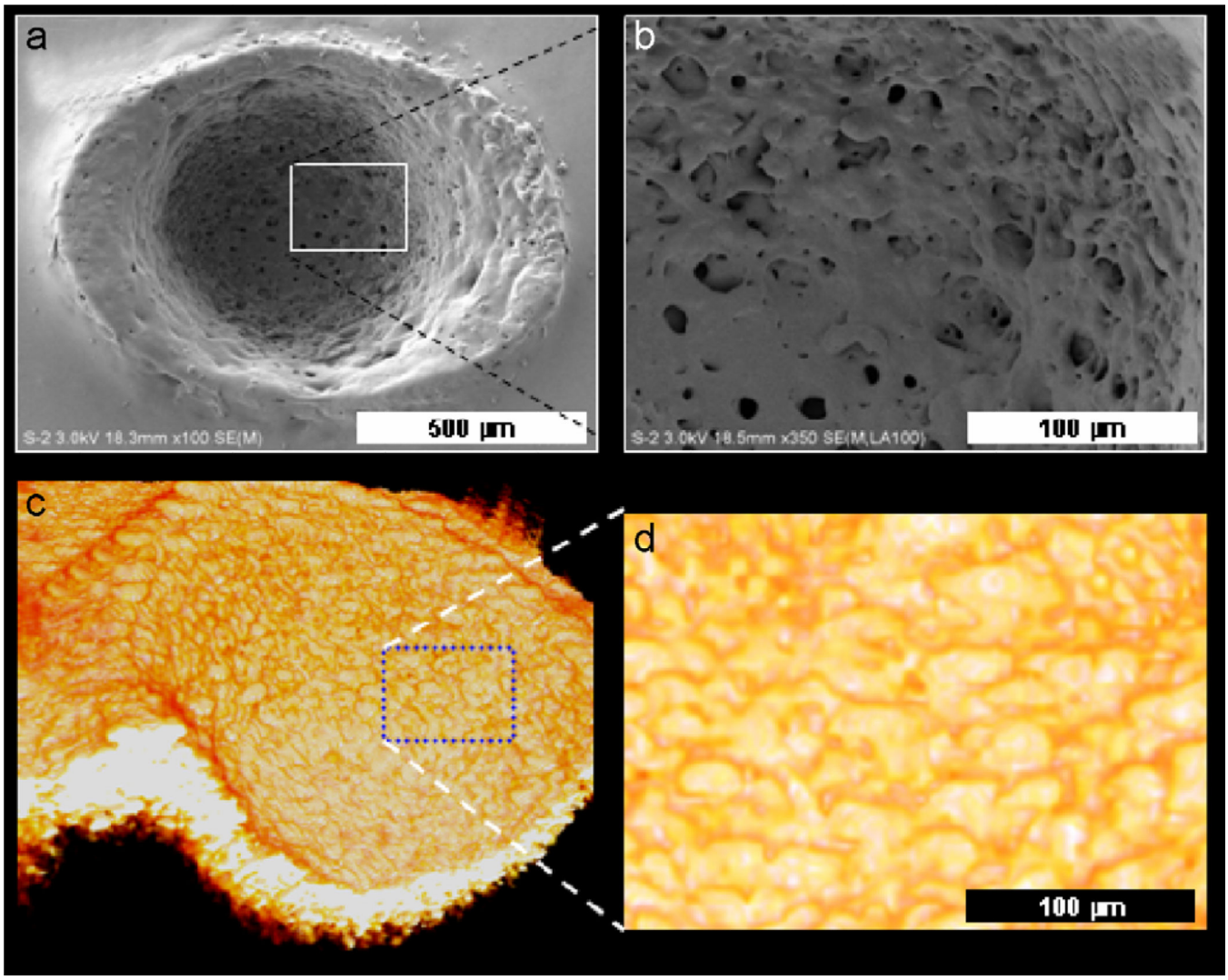

Fig. 7.

Comparison of SEM images with OCT images to show the detailed information of the deformed surface morphology. (a) The top view and (b) the bottom view SEM images. The OCT images of (c) the three-dimensional view of the pit and (d) the magnified view presenting the detailed surface roughness of the pit. For pit creation, an ABS plastic was used under the laser operational condition of 40 pulses at 20 Hz.